6 Drag in Double-Layer Systems

The advent of sophisticated epitaxial growth techniques has enabled the fabrication of double-layer (or, more generally, multi-layer) GaAs/AlGaAs quantum well heterostructures and opened the road towards an investigation of the interaction between two or multiple 2DEGs. When two parallel 2DEGs are brought into close proximity, a current in one of the layers is able to induce a response in the other layer.[1] This effect is due to interaction between the electrons in the active (current-carrying) and the passive (responding) layer and was first predicted in a semiconductor-insulator-semiconductor system by Pogrebinskii [79] and in heterolayer structures by Price [80]. In general, the response of the passive layer consists of a current, which is induced by the electrons of the active layer through Coulomb and/or electron-phonon interaction. Naively, one would expect – on the basis of momentum conservation – that the electrons in the active layer "drag along" the electrons in the passive layer, leading to a current which points in the same direction as that in the active layer, hence the name of the effect: "drag". If the current induced in the passive layer flows in the same direction as the current in the active layer, one speaks of *positive* drag.

Although this simple scenario is valid in numerous situations, there are situations for which this picture ceases to hold true. By applying a perpendicular magnetic field to the bilayer system, the behavior of drag can be changed dramatically. A prominent example is the case of two quantum Hall layers close to half filling, which form a new, strongly correlated ground state reminiscent of an excitonic condensate [81]. Another example is the oscillating sign of drag observed in high Landau levels at sufficiently low temperatures. This anomalous drag effect was subject to a number of experimental studies [82, 83, 84] and can be explained as an effect of different fillings of the two layers [85, 86, 87].

The information provided by drag measurements in a perpendicular magnetic field is complementary to conventional transport measurements and thus constitutes a valuable additional tool for the investigation of quantum Hall systems. It directly probes the electron-electron interaction between different layers and provides information about inelastic scattering and correlations between the layers. Most experimental and theoretical work is focused on the study of Coulomb drag, i.e. the effect of Coulomb interlayer interactions, which is dominant for small interlayer separations d. For larger d, the effect of the Coulomb interaction gets weaker up to a point where also phonon interaction or other types of interaction might become relevant.

In what follows, we first address a number of important conventions adopted when talking about drag phenomena (Section 6.1). We then discuss the state of

[1] The interlayer spacing should still be large enough to prevent direct charge transfer between the two subsystems by tunneling.

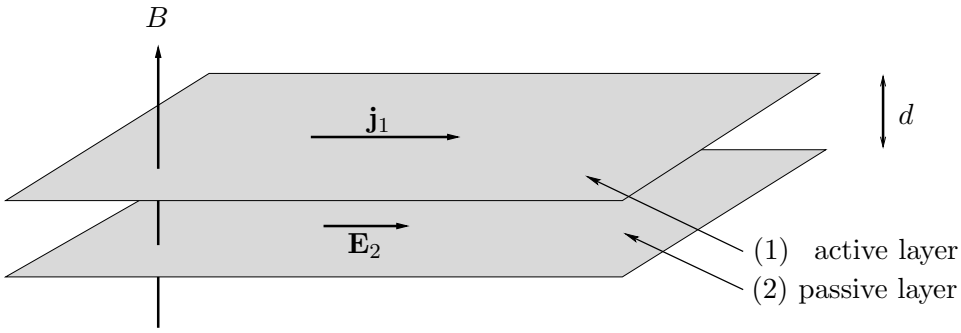

Figure 6.1: Sketch of a double layer system. The two parallel layers, separated by a distance d, behave as 2DEGs. Drag experiments are carried out in systems of this type by applying a current to one of the layers and measuring the induced current in the other layer (or, equivalently, the induced voltage in an open-circuit setup).

experiment and theory of Coulomb drag in Section 6.2, focussing on the oscillating sign of drag for two 2DEG layers of mismatched densities. In Section 6.3, we provide a brief introduction to phonon drag. Section 6.4 introduces the linear response theory for frictional drag. All considerations serve as background for our study of phonon drag in high Landau levels presented in Chapter 7. Technical details, such as the analytical continuation of the drag conductivity and the so-called triangle vertices, as well as an introduction to the self-consistent Born approximation (SCBA) are deferred to Appendices A-D.

6.1 Conventions

Conventionally, drag experiments on double-layer systems are carried out in an open-circuit setup, which differs slightly from the simple picture discussed above. Instead of a current, a voltage V develops in the passive layer to balance the momentum transfer from the active layer. For like (unlike) charges of the current carriers in both layers, the voltage sign in the passive layer is expected to be opposite (equal) to that of the voltage in the active layer. In accordance with the convention adopted in the literature, we refer to the sign resulting for like (unlike) charges as positive (negative) drag.

In this way, the drag resistivity (or transresistivity) is defined as

$$\rho_{ij}^D = -\frac{E_{2,i}}{j_{1,j}} \quad , \tag{6.1}$$

where the indices $1, 2$ label the layers and i, j the cartesian x- and y-components. j_1 denotes the current in the active layer and E_2 the induced electric field in the passive layer. Within the Kubo formalism, it is more convenient to study the drag conductivity

$$\sigma_{ij} = -\frac{j_{2,i}}{E_{1,j}} \quad . \tag{6.2}$$

Experiments, in turn, usually measure the dc drag resistivity ρ_{ij}^D, which is related to the drag conductivity via

$$\rho_{ij}^D = \rho_{ik}^{(1)} \; \sigma_{kl}^D \; \rho_{lj}^{(2)} \quad , \tag{6.3}$$

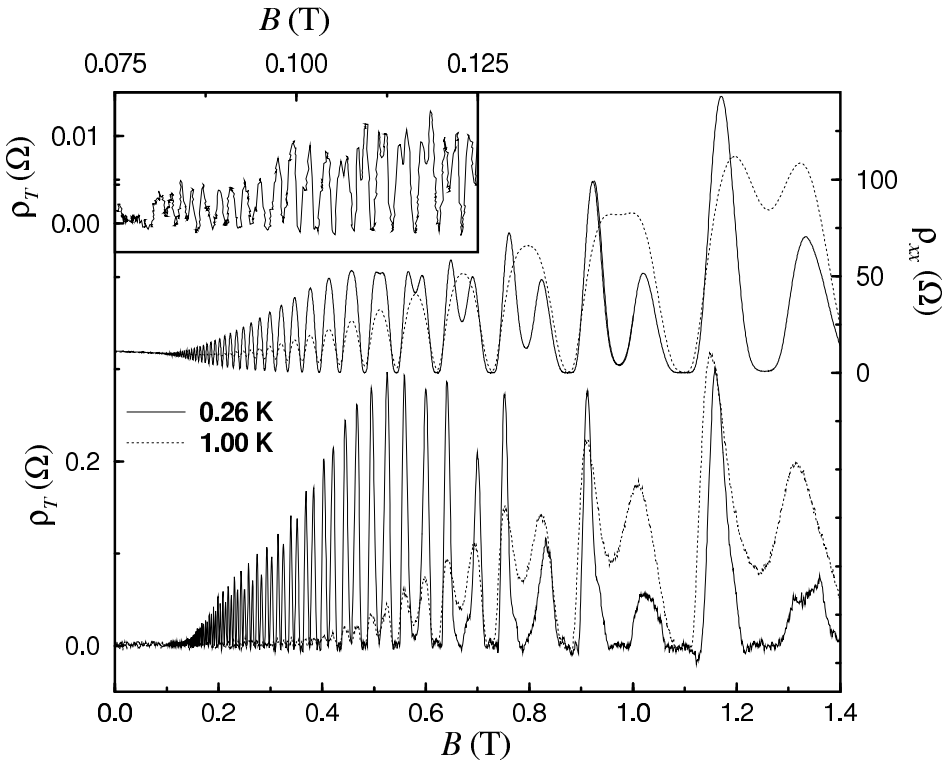

Figure 6.2: Drag resistivity (or transresistivity) ρ_T (bottom curve) and diagonal resistivity ρ_{xx} (top curve) as a function of magnetic field B for matched densities of the two 2DEG layers ($n_1 = n_2 = 2.13 \times 10^{11}$ cm^{-2}) from an experiment in high LLs by Lok *et al.* [83]. The curves were taken at temperatures $T = 0.26$ K (solid lines) and $T = 1$ K (dotted lines). The inset shows ρ_T at the lower temperature, $T = 0.26$ K, and the appearance of spin-split double-peak structures for magnetic fields $B \gtrsim 0.11$ T. This figure has been taken from Ref. [83].

where $\rho_{ik}^{(1)}$ and $\rho_{ik}^{(2)}$ are the usual resistivities of the two layers.[2]

The main parameters governing the drag response of a double-layer system are:

- the interlayer spacing d, controlling the strength of the interlayer interaction,
- the charges q_1, q_2 (and, possibly, the spins) of the carriers in active and passive layers,
- the carrier densities n_1, n_2 and, in a perpendicular magnetic field, the LL filling factors ν_1, ν_2 of the two layers.

[2]The usual minus sign corresponding to standard tensor inversion is absent in this expression due to our specific choice of sign conventions. Based on this, the transresistivity is positive in the absence of a magnetic field.

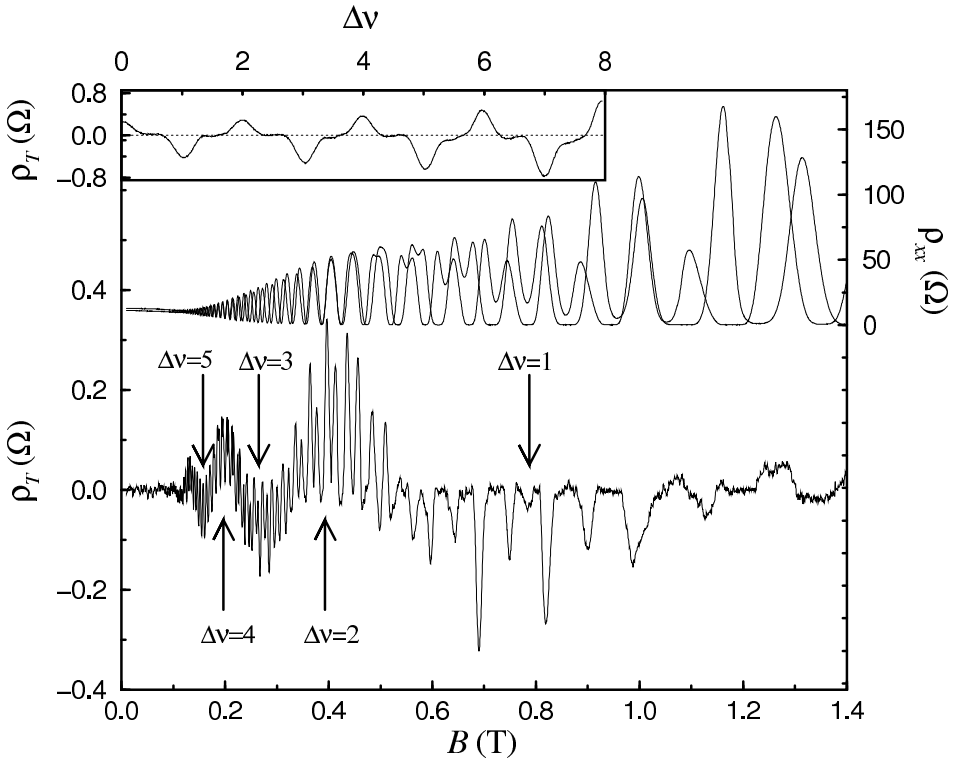

Figure 6.3: Drag resistivity (or transresistivity) ρ_T (bottom curve) and diagonal resistivity ρ_{xx} (top curve) as a function of magnetic field for mismatched densities of the two 2DEG layers ($n_1 = 2.27 \times 10^{11}$ cm^{-2}, $n_2 = 2.08 \times 10^{11}$ cm^{-2}) from an experiment by Lok *et al.* [83] at $T = 0.25$ K. The inset shows the transresistivity at fixed magnetic field $B = 0.641$ T as a function of filling-factor difference $\Delta\nu$. This figure has been taken from Ref. [83].

6.2 Coulomb Drag

In the regime of high Landau levels, the sign of the drag resistivity depends on whether the densities of the two 2DEG layers are matched ($n_1 = n_2$) or mismatched ($n_1 \neq n_2$). These two cases are shown in Figs. 6.2 and 6.3, respectively. For matched densities, the drag resistivity ρ_D (denoted by ρ_T in the figures, the subscript T denoting the *trans*resistivity) is always positive (see Fig. 6.2). For increasing magnetic field, Fig. 6.2 shows the usual Shubnikov-deHaas oscillations in the diagonal resistivity ρ_{xx} for magnetic fields $B \gtrsim 0.1$ T. Spin-splitting of these oscillations is resolved at magnetic fields $B \gtrsim 0.5$ T. The drag resistivity is roughly two orders of magnitude smaller than the diagonal resistivity. As shown in the inset of Fig. 6.2, which details the behavior of ρ_T at low magnetic fields, spin-splitting in ρ_T sets in for considerably lower magnetic fields ($B \gtrsim 0.11$ T) than in ρ_{xx}.

In the case of mismatched layer densities, shown in Fig. 6.3, the drag resistivity assumes positive and negative values, the sign varying in an oscillatory manner as a function of the inverse magnetic field. These slow oscillations are accompanied by fast oscillations reflecting the underlying LL density of states.

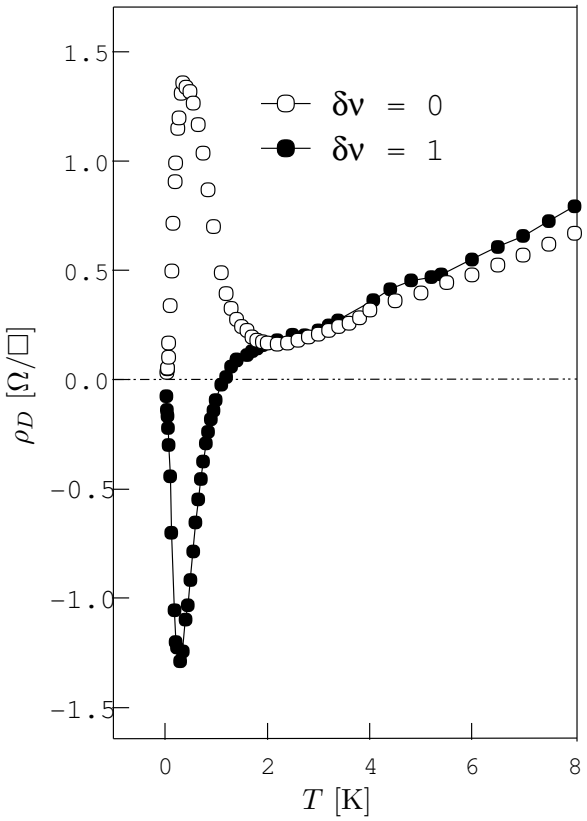

Figure 6.4: Temperature dependence of drag from an experiment by Muraki *et al.* [84]. Strong deviations from the monotonic T^2-dependence expected for ideal Fermi liquids are observed. As opposed to matched layer densities ($\delta\nu = 0$), the sign of drag may change with temperature at mismatched densities ($\delta\nu \neq 0$). This figure is a modified version of a figure taken from Ref. [84].

Positive maxima appear whenever the filling factor difference $\Delta\nu$ between the two 2DEG layers is even, while negative minima appear when it is odd. This behavior is emphasized in the inset of Fig. 6.3 which shows the filling factor dependence of the drag resistivity for fixed magnetic field.

The dependence of the drag resistivity on the filling factor of the topmost filled LLs has been studied experimentally by Feng *et al.* [82], who find positive drag when the topmost LLs in both layers are either both more than half filled or less than half filled and negative drag if one is more and the other less than half filled.

It is interesting to study the temperature dependence of drag. If the scattering took place between two layers behaving as ideal Fermi liquids, the temperature dependence of the drag resistance would be monotonic and behave as

$$R_D \propto T^2 \quad ,$$

since the available phase space for interlayer scattering would be proportional to T in either layer. In particular, since the available phase space for electron-electron scattering tends to zero at low temperatures, Coulomb drag is expected

to decrease with decreasing temperature.

There are, however, important deviations from this behavior [88]. In high magnetic fields, there are strong deviations from this temperature dependence, consisting of nonmonotonic behavior of $\rho_D(T)$ [84]. In addition, depending on the matching of the layer densities, the sign of the drag resistivity may also change with temperature as depicted in Fig. 6.4. Apparently, the temperature dependence is nonmonotonic and deviates strongly from the T^2-behavior predicted by the simplified consideration above.

Historically, the theoretical investigation of drag initially was centered on Coulomb drag in coupled electron systems in the *absence* of a magnetic field [89]. Coulomb drag can be treated within linear response theory. It can be shown that the Coulomb drag conductivity is governed by momentum transfers $q < 1/d$. This is due to the specific form of the interlayer Coulomb interaction,

$$U(q) \propto \frac{\exp(-qd)}{q^2} \quad , \tag{6.4}$$

which is suppressed at large momenta by a factor $\exp(-qd)$. Recently, considerations were expanded to the case of Coulomb drag at finite magnetic fields [85, 86].

6.3 Phonon Drag

For large interlayer separations, the Coulomb interaction, Eq. (6.4), is suppressed and additional mechanisms of interlayer momentum transfer become more important. Fig. 6.5 shows experimental results for the total drag scattering rate[3] as a function of temperature (scaled by T^{-2}) in a sample with rather large interlayer separation (at zero magnetic field). The dashed line in Fig. 6.5 indicates the expected contribution from Coulomb drag,[4] which by itself is unable to account for the observed temperature dependence. The weak dependence of the additional contribution to the total drag scattering rate on interlayer separation, depicted in the inset of Fig. 6.5, strongly suggests phonon-mediated interlayer interactions. This additional mechanism of interplay between the two layers of a bilayer system is known as *phonon* drag [90] and has been studied at zero magnetic field in Ref. [91]. It stems from the indirect interaction of electrons in the two layers via bulk phonons. In Chapter 7, we will study phonon drag in finite magnetic fields, more precisely in the regime of high Landau levels.

The most striking observation in Ref. [90] is a distinct peak in the temperature dependence of phonon drag near $T = 2$ K, which, qualitatively, can be understood as follows. At low temperatures T, only phonons with small wave

[3] The drag scattering rate τ_D^{-1} is closely related to the drag resistance R_D via

$$R_D = -\frac{L}{W}\frac{m}{ne^2}\,\tau_D^{-1} \quad ,$$

where L and W are length and width of the sample, m is the effective electron mass, and n the electron density in the active layer [88].

[4] This contribution is constant, due to the T^{-2}-scaling.

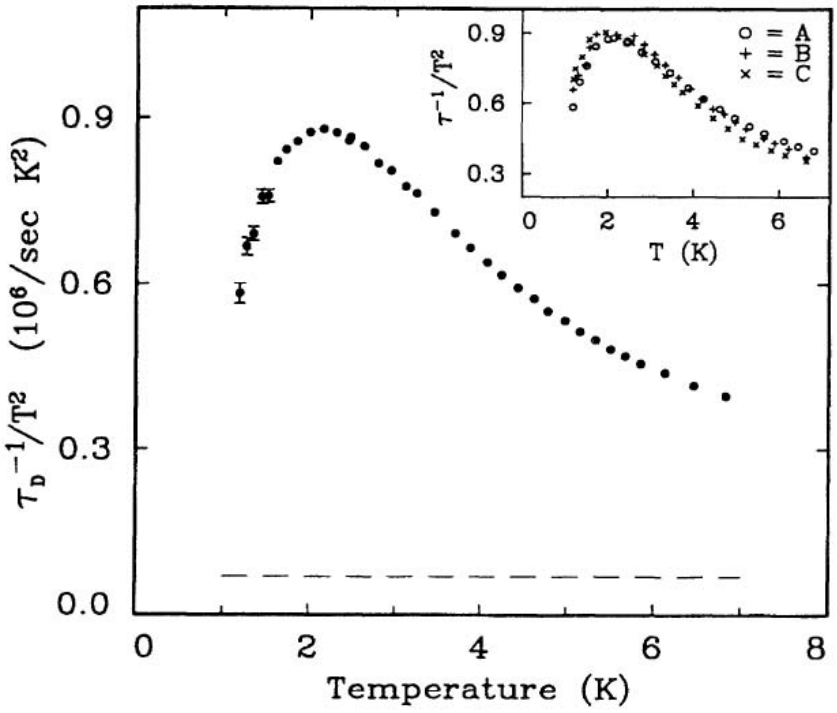

Figure 6.5: Measured temperature dependence of the drag scattering rate τ_D^{-1}, scaled by T^2, for a double-quantum-well sample with interlayer separation of 500 Å in absence of a magnetic field from an experiment by Gramila and co-workers [90]. The dashed line denotes the estimated Coulomb contribution, indicating that Coulomb interactions alone are unable to account for the temperature dependence of drag. The inset shows results for the additional contribution to τ_D^{-1}/T^2 at three different interlayer separations (500 Å (A), 225 Å (B), and 175 Å (C)). Here, the (spacing-dependent) contribution of Coulomb drag to τ_D^{-1}/T^2 has been subtracted for all three interlayer separations. The dependence of the additional contribution on interlayer separation turns out to be very weak. This points towards phonon interlayer interactions as the possible source of the additional contribution. This figure has been taken from Ref. [90].

vectors $q < 2k_F$ can be thermally excited and participate in the interlayer momentum transfer. As T increases, phonon states with higher wave vectors become occupied, leading to larger momentum transfers and, simultaneously, opening access to a larger portion of the electron phase space. This leads to an increase of phonon drag. The strong increase continues until phonons with wave vector $q \sim 2k_F$ can be thermally excited. Since, to lowest order in the phonon-mediated interaction, there are no scattering processes involving phonons of momenta $q > 2k_F$, the increase of phonon drag is slowed down at higher temperatures. The temperature at which the transition between these two behaviors takes place can be determined from the condition $q \sim 2k_F$ together with the phonon dispersion $\omega = cq$, where c is the phonon velocity. Equating the typical phonon frequency with the temperature, this yields $T_{bs} = 2ck_F$, the subscript bs standing for backscattering, since a momentum transfer of $2k_F$ corresponds to complete momentum inversion of the scattered electron.

As for Coulomb drag, the theoretical description of phonon drag relies on linear response theory. In contrast to Coulomb drag, as evident from the previous considerations, the momentum transfer in phonon drag is not restricted to small momenta. We therefore have to generalize the theory of Coulomb drag to arbitrary momentum transfers. In Chapter 7, we will demonstrate that phonon scattering indeed affects frictional drag predominantly at temperatures in the vicinity of $T_{bs} = 2ck_F$, and that the main contribution to phonon drag is due to momenta $q \lesssim 2k_F$.

6.4 Linear Response Theory of Drag

In this section, we describe the linear response theory of frictional drag.[5] It is based on the theory of Coulomb drag in high Landau levels [86] and will be generalized to the treatment of phonon drag in the present thesis.

6.4.1 Drag Conductivity

Within the Kubo formalism, the dc drag conductivity σ_{ij}^D can be written in terms of a current-current correlation function (see Appendix A), which, after analytical continuation (see Appendix B), evaluates to

$$\sigma_{ij}^D = \frac{e^2}{16\pi TS}\sum_{\mathbf{q}}\int_{-\infty}^{\infty}\frac{d\omega}{\sinh^2\left(\frac{\omega}{2T}\right)}\Bigg\{\Gamma_i^{(1)}(\mathbf{q},\omega+i0,\omega-i0) \times\Gamma_j^{(2)}(\mathbf{q},\omega-i0,\omega+i0)|W(\mathbf{q},\omega)|^2\Bigg\} \quad . \tag{6.5}$$

Here, T is the temperature, S is the area of the sample and $W(\mathbf{q},\omega)$ is the interlayer interaction, which is assumed to be weak and might be screened. In Eq. (6.5), the vector $\mathbf{\Gamma}^{(l)}(\mathbf{q},\omega) \equiv \Gamma^{(l)}(\mathbf{q},\omega+i0,\omega-i0)$ denotes the so-called triangle vertex of layer l as defined by the sum of the two diagrams in Fig. 6.6.

6.4.2 Triangle Vertex

We now turn to the evaluation of the disorder-averaged triangle vertex $\mathbf{\Gamma}(\mathbf{q},\omega)$. The result of the analytical continuation (see Appendix C) of the triangle vertex can be written as

$$\mathbf{\Gamma} = \mathbf{\Gamma}^{(a)} + \mathbf{\Gamma}^{(b)} \quad , \tag{6.6}$$

[5] *Frictional drag* is a term often used to describe the entirety of drag phenomena irrespective of the underlying mechanism (e.g., Coulomb or phonon-mediated interactions).

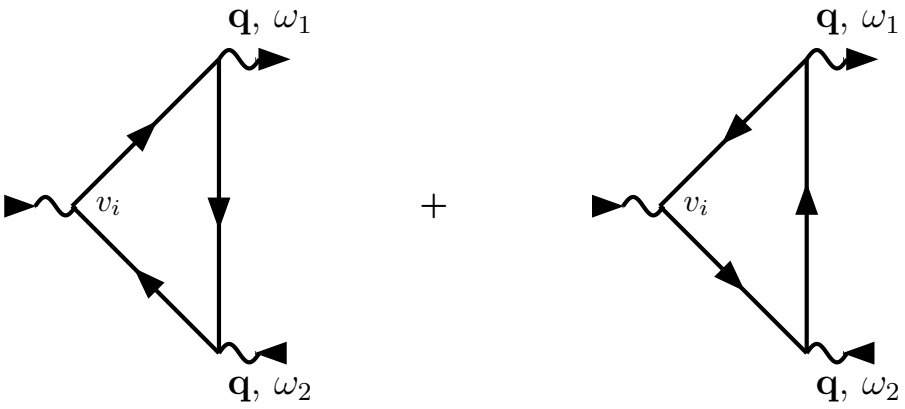

Figure 6.6: Diagrams defining the three-leg triangle vertex $\mathbf{\Gamma}(\mathbf{q}, \omega_1, \omega_2)$. The vector (current) vertices are labeled by the velocity operator v_i. This figure has been taken from Ref. [86].

where

$$\begin{aligned}\mathbf{\Gamma}^{(a)}(\mathbf{q},\omega) = \int \frac{d\epsilon}{4\pi i} \tanh\left(\frac{\epsilon+\omega-\mu}{2T}\right) \\ \times \mathrm{tr}\Big\{\mathbf{v}\mathcal{G}^+(\epsilon+\omega)e^{i\mathbf{qr}}\mathcal{G}^+(\epsilon)e^{-i\mathbf{qr}}\mathcal{G}^+(\epsilon+\omega) \\ - \mathbf{v}\mathcal{G}^-(\epsilon+\omega)e^{i\mathbf{qr}}\mathcal{G}^-(\epsilon)e^{-i\mathbf{qr}}\mathcal{G}^-(\epsilon+\omega)\Big\} \\ + (\omega, \mathbf{q} \to -\omega, -\mathbf{q}) \quad , \end{aligned} \tag{6.7}$$

and

$$\begin{aligned}\mathbf{\Gamma}^{(b)}(\mathbf{q},\omega) = \int \frac{d\epsilon}{4\pi i} \left[\tanh\left(\frac{\epsilon+\omega-\mu}{2T}\right) - \tanh\left(\frac{\epsilon-\mu}{2T}\right)\right] \\ \times \ \mathrm{tr}\left\{\mathbf{v}\mathcal{G}^-(\epsilon+\omega)e^{i\mathbf{qr}}[\mathcal{G}^-(\epsilon) - \mathcal{G}^+(\epsilon)]e^{-i\mathbf{qr}}\mathcal{G}^+(\epsilon+\omega)\right\} \\ + (\omega, \mathbf{q} \to -\omega, -\mathbf{q}) \quad . \end{aligned} \tag{6.8}$$

Here, $\mathcal{G}^{\pm}(\epsilon) \equiv \mathcal{G}(\epsilon \pm i0)$ are the advanced and retarded electron Green functions for a specific realization of the disorder potential, respectively, and $\mathbf{v}$ is the velocity operator.

6.4.3 Triangle Vertex in the Low Temperature Limit

We are interested specifically in the drag conductivity in the low temperature limit $T, \omega \ll \Delta \ll \omega_c$, where Δ is the Landau level broadening (see Appendix D).[6] In this low temperature limit, the ϵ-integration in Eqs. (6.7-6.8) is trivial[7]

[6] Note that in previous chapters, the Landau level broadening was denoted by Γ. We chose to shift our notation to Δ to avoid confusion with the triangle vertex denoted by $\mathbf{\Gamma}$.

[7] In the low temperature limit, the traces in Eqs. (6.7-6.8) do not depend on the integration variable ϵ and can thus be evaluated at $\epsilon = E_F$.

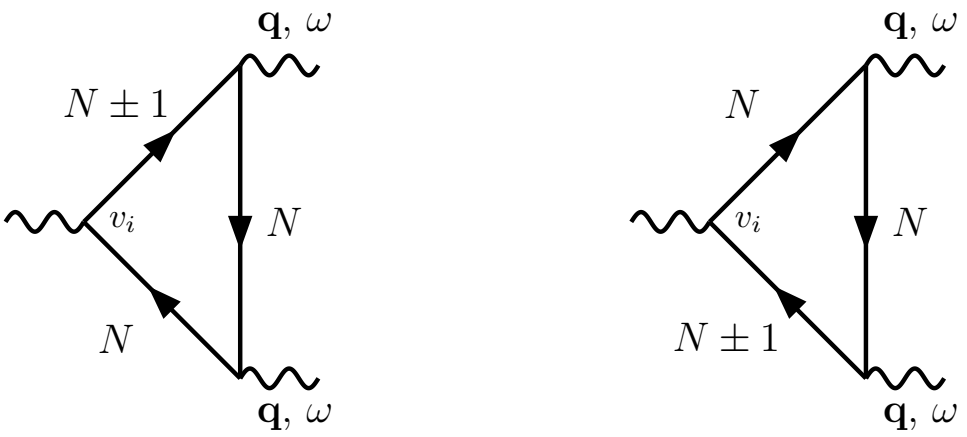

Figure 6.7: The diagrams contributing to the triangle vertex within SCBA to leading order in the limit of well-separated Landau levels $\Delta/\omega_c \ll 1$ and large N. This figure has been taken from Ref. [86].

and the two contributions to the triangle vertex simplify to

$$\begin{aligned}\mathbf{\Gamma}^{(a)}(\mathbf{q},\omega) &= \frac{\omega}{2\pi i}\mathrm{tr}\Big\{\mathbf{v}\mathcal{G}^+(E_F)e^{i\mathbf{qr}}\mathcal{G}^+(E_F)e^{-i\mathbf{qr}}\mathcal{G}^+(E_F) \\ &\qquad -(\mathcal{G}^+\to\mathcal{G}^-)\Big\} \quad , \qquad (6.9)\\ \mathbf{\Gamma}^{(b)}(\mathbf{q},\omega) &= \frac{\omega}{i\pi}\mathrm{tr}\Big\{\mathbf{v}\mathcal{G}^-(E_F)e^{i\mathbf{qr}}[\mathcal{G}^-(E_F)-\mathcal{G}^+(E_F)]e^{-i\mathbf{qr}}\mathcal{G}^+(E_F)\Big\}. \qquad (6.10)\end{aligned}$$

Here, E_F is the Fermi energy (or chemical potential) located in the Nth LL. The disorder-averaging of the triangle vertex $\mathbf{\Gamma}$ is performed within the self-consistent Born approximation (SCBA, see Appendix D) . The calculation of the traces appearing in the above expressions involves matrix elements (between LL eigenstates) of the impurity-averaged Green functions (which are diagonal in the Landau gauge) and of $e^{i\mathbf{qr}}$ and the velocity operator $\mathbf{v}$ (see Appendix D). To leading order in Δ/ω_c, two of the three Green functions in Eqs. (6.9-6.10) have to be evaluated in the Nth Landau level in which the Fermi energy is situated.[8] However, since the velocity operator has matrix elements only between states in neighboring Landau levels,

$$\begin{aligned}\langle nk|v_x|n\pm 1k'\rangle &\simeq \mp i\delta_{kk'}\frac{v_F}{2} \quad , \qquad (6.11)\\ \langle nk|v_y|n\pm 1k'\rangle &\simeq \delta_{kk'}\frac{v_F}{2} \quad , \qquad (6.12)\end{aligned}$$

one of the Green functions adjacent to the vector vertex must be taken in Landau levels $N\pm 1$, as illustrated in Fig. 6.7.

We find that $\mathbf{\Gamma}^{(a)}$ gives a purely longitudinal contribution (parallel to $\mathbf{q}$) to the triangle vertex. To see that the transverse contribution to $\mathbf{\Gamma}^{(a)}$ indeed vanishes, one can use the fact that $\mathbf{\Gamma}^{(a)}(\mathbf{q},\omega)$ can be expressed as (see Eq. (C-9))

$$\mathbf{\Gamma}^{(a)}(\mathbf{q},\omega) = \frac{\omega}{\pi}\nabla_{\mathbf{q}}\mathrm{Im}\,\mathrm{tr}\left\{e^{i\mathbf{qr}}\mathcal{G}^+(E_F)e^{-i\mathbf{qr}}\mathcal{G}^+(E_F)\right\} \quad . \qquad (6.13)$$

[8] This is due to the fact that matrix elements of Green functions outside the Nth Landau level are smaller by a factor of $1/\omega_c$.

Eq. (6.13) can be derived by noting that

$$\nabla_{\mathbf{q}} \mathrm{tr}\left\{e^{i\mathbf{qr}}\mathcal{G}^{+}e^{-i\mathbf{qr}}\mathcal{G}^{+}\right\} = i\mathrm{tr}\left\{e^{i\mathbf{qr}}\left[r,\mathcal{G}^{+}\right]_{-}e^{-i\mathbf{qr}}\mathcal{G}^{+})\right\} \tag{6.14}$$

and using the fact that

$$\left[r,\mathcal{G}^{+}\right]_{-} = \frac{\partial}{\partial q}\mathcal{G}^{+} = \mathcal{G}^{+}v\mathcal{G}^{+} \quad . \tag{6.15}$$

The trace in Eq. (6.13) only depends on the absolute value of $\mathbf{q}$, and thus the gradient with respect to $\mathbf{q}$ ensures that $\mathbf{\Gamma}^{(a)}$ is parallel to $\mathbf{q}$. By contrast, $\mathbf{\Gamma}^{(b)}$ generally yields both longitudinal and transverse contributions to the triangle vertex.